An Optical Ray Tracer

Gerry O'Brien

I. Introduction

I aimed to use object orientated programming to simulate the propagation of rays through a spherical refracting surface and then use this to investigate the imaging performance of plano-convex lenses in different orientations.

II. The Single Spherical Refracting Surface

I set up the 'SphericalRefraction' class, inherited from 'OpticalElement', with parameters: z0 - the position of the lens on the z-axis (with the rays always starting at z = 0), curvature - 1/radius of sphere, n1 and n2 – the refractive indices before and after the surface, and the aperture radius.

Initially I had to write a method for finding the intercept of a ray with a spherical surface. To do this I had to consider situations with zero curvature (a flat surface) and positive and negative curvature separately as I only wanted to find the first intersection with the sphere. I did this using the diagram and equations from the project script. Positive curvature was set as in the diagram. Furthermore, I ensured that python returned 'None' if there was no point of intersection with the surface which I tested by propagating a few rays that I knew wouldn't intersect through the ray tracer.

The next step was implementing Snell's Law to find the direction of a ray after refraction through the spherical surface. The vector form of Snell's Law is,

$$\boldsymbol{t} = \mu \boldsymbol{i} + \boldsymbol{n}\sqrt{1-\mu^2(1-(\boldsymbol{n}\cdot\boldsymbol{i})^2)} - \mu\boldsymbol{n}(\boldsymbol{n}\cdot\boldsymbol{i}) \quad (1)[1]$$

where μ is n1/n2, **i** is the incident ray's directional unit vector, **t** is the directional unit vector after refraction and **n** is the normal to the surface, shown in figure 1.

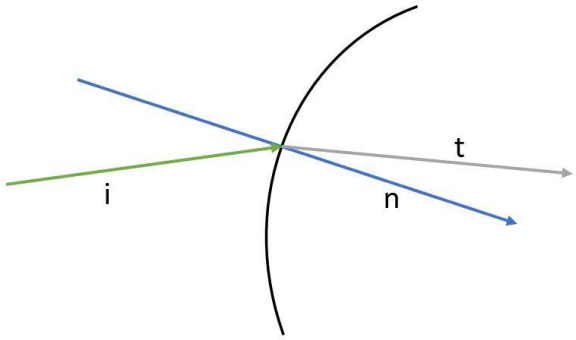

Figure 1 - Diagram showing the directions of the relevant vectors used in Snell's Law

Again, it was important to consider the three cases (zero curvature, positive curvature, and negative curvature) separately as the normal vector I needed for equation 1 was different in each case. For the flat surface case the unit normal vector was just +1 in the z direction. For both positively and negatively curved spherical surfaces I set the normal to point towards the centre of the sphere. This meant I had to use the negative of the normal found for the negative curvature as the centre of the sphere was between the input and the surface and it was vital, for the refraction to work, that the normal always points away from the input of the rays. I forced the method to return 'None' if total internal reflection should occur.

To propagate the ray I created a method which appended a new position and direction to a previously created list containing the original position and direction of the ray, set in the Ray class. The new position was the intercept of the ray with the surface and the new direction was found using the 'SnellsLaw' method. I then plotted the positions of a few rays to visualize the propagation and check the refractor was working.

To fully propagate the rays, I needed to create an output plane for the rays to intersect with. Initially I did this by creating a method within the 'SphericalRefraction' class automatically propagating every ray to the output plane when a ray was propagated through a spherical refracting surface. This broke down when I tried to propagate a ray through more than one surface. I realised that I needed to make the output plane its own class which used a method to find the intercept of a ray with the plane and appended that position to the list of vertices upon propagation.

III. Testing the Single Spherical Refracting Surface within the Paraxial Limit

I considered paraxial rays when first testing the spherical refracting surface because this minimises the spherical and chromatic aberrations due to refraction in a spherical surface, which increase as the ray gets further from the optical axis. It is also a good approximation for a point light source at infinity.

For all tests on the single spherical refracting surface I used the parameters shown in table 1.

Parameter	z0 / mm	Curvature / mm^{-1}	n1	n2	Aperture radius / mm
Value	100	0.03	1.0	1.5	10

Table 1 - The parameters on the single spherical refracting surface

I traced 11 paraxial rays all within a millimeter of the optical axis. From figure 2, I could see that the focal length was about 100 mm.

	Theoretical	Calculated
Focal length / mm	100.0000	99.9998

Table 2 - The theoretical and calculated focal lengths for the single spherical refractor

I got an accurate value for the paraxial focal length by tracing a single ray, 0.1 mm from the optical axis, through the refractor and calculating where it crossed the optical axis after refraction. I compared this to the theoretical focal length which I calculated using the equation for the focal length of a spherical lens,

$$f = \frac{n_2}{curvature(n_2 - n_1)} \quad (2)[2]$$

where f is the focal length, and n_1 and n_2 are the refractive indices before and after the surface.

As shown in table 2, the paraxial focal length I found using my surface was only out by a factor of 10^{-4} mm suggesting the surface refracts accurately within the paraxial limit.

I tested whether the spherical surface could be used as an approximation for a thin lens, which uses two spherical surfaces. I did this by creating a point source one focal length from the surface, and observing the propagation of the rays, shown in figure 3. I decided that it was a bad approximation for a thin lens because the thin lens would've refracted the rays to travel parallel to the optical axis whilst my surface refracted the rays to a rough focal point about 290 mm from the surface.

IV. Testing the Single Spherical Refracting Surface beyond the Paraxial Limit

The next step was testing the single spherical refracting surface beyond the paraxial limit. To do this I attempted to make a uniform collimated beam consisting of many rays evenly distributed across a circle. I made a function which plotted out points on concentric circles with the radius and number of concentric circles controlled by the arguments, 'R' and 'n_step'. It plotted evenly spaced points around each concentric circle, also controlled by 'n_step', before stepping out to the next circle.

For this test I used a bundle of radius of 2.5 mm with 8 steps as this appeared to be the best model for a fairly uniform distribution and provided enough data points to take good averages. This is shown in figure 4. After moving the output plane to the paraxial focal length, I propagated the collimated beam through the single spherical refracting surface, as seen in figure 5. The spot diagram at the paraxial focal length, in figure 6, shows that the rays closer to the optical axis were refracted closer to the focal point.

The project script suggested finding the root-mean-square deviation of the ray positions from the optical axis to use as the geometrical focus size.

Focus size / mm	Diffraction limit (λ=588nm) / mm
0.0014	0.0118

Table 3 - The focus size for a 2.5mm radius beam and the diffraction limit of light with a wavelength of 588 nm refracting in the spherical surface

I calculated the diffraction limit using the equation from the project script and assumed a wavelength of 588 nm. Looking at table 3, the focus size is about a tenth of the diffraction limit which means the refractor's maximum resolving power, for this particular beam, is limited by the diffraction limit [3] rather than spherical aberrations.

V. Modelling a Plano-Convex Singlet Lens

Simple plano-convex lenses often use a flat surface and a spherical surface as spherical surfaces are fairly easy and cheap to make. This meant I could use my spherical refractor to model this lens with a spherical surface and a zero-curvature surface.

It was possible to make a plano-convex singlet lens with a focal length of about 100 mm with glass of refractive index 1.5168 and a convex side with curvature of 0.02 mm^{-1}. I tested this lens with both the flat side facing the input and the convex side facing the input. I chose to find the size of the focus for a range of beam diameters but I have only included the plots for the maximum beam diameter (10 mm), with its spot diagram at the input shown in figure 7, as this is the one with the most spherical aberration so is the most likely to have its focus size outweigh the diffraction limit.

I considered the flat side towards the input as the first case and the curved side towards the input as the second case.

Beam Diameter / mm	Focus size, 1st case / mm	Focus size, 2nd case / mm	Diffraction limit / mm
2	0.00021	0.00005	0.0294
4	0.00169	0.00043	0.0147
6	0.00573	0.00144	0.00980
8	0.01363	0.00343	0.00735
10	0.02674	0.00671	0.00588

Table 4 - The focus sizes for both orientations of the plano-convex lens for a range of beam diameters

After propagation through the plano-convex lenses, shown in figures 8 and 10, to generate the spot diagrams, shown in figures 9 and 11, I had to find new paraxial focal lengths, still using a single ray 0.1 mm from the optical axis but this time propagating through two surfaces. I got the values: 101.7 mm for the first case and 98.5 mm for the second case. This suggested that the lens behaves slightly differently in each case.

The focus sizes for the first case are between 4 and 5 times larger than the focus sizes for the second case, seen in table 4. The lens performed a lot better with the convex side facing the input. This is because the convex surface introduces spherical aberrations so it should be providing less refracting power than the flat surface to minimize this. This is achieved by allowing the ray to pass through the convex surface first.

As the diameter of the beam was increased, in the first case the focus size becomes larger than the diffraction limit at 8 mm diameter. In the second case the focus size becomes larger than the diffraction limit by only about 10^{-3} mm at 10 mm diameter. These are the rough points at which the maximum resolving power becomes limited by spherical aberrations more than the diffraction limit.

References

[1] Physics Stack Exchange. (2018) *Snell's Law in Vector Form.* https://physics.stackexchange.com/questions/435512/snells-law-in-vector-form#:~:text=where%20%CE%B81%20is%20the,optical%20medium%20behind%20the%20interface. [Accessed 01/11/2021]

[2] MIT. (2005) Lenses and Imaging Part 1. [Presentation] MIT, 14th September.

[3] Edmund Optics. (n.d.) The Airy Disc and Diffraction Limit. https://www.edmundoptics.co.uk/knowledge-center/application-notes/imaging/limitations-on-resolution-and-contrast-the-airy-disk/ [Accessed 06/12/2021]

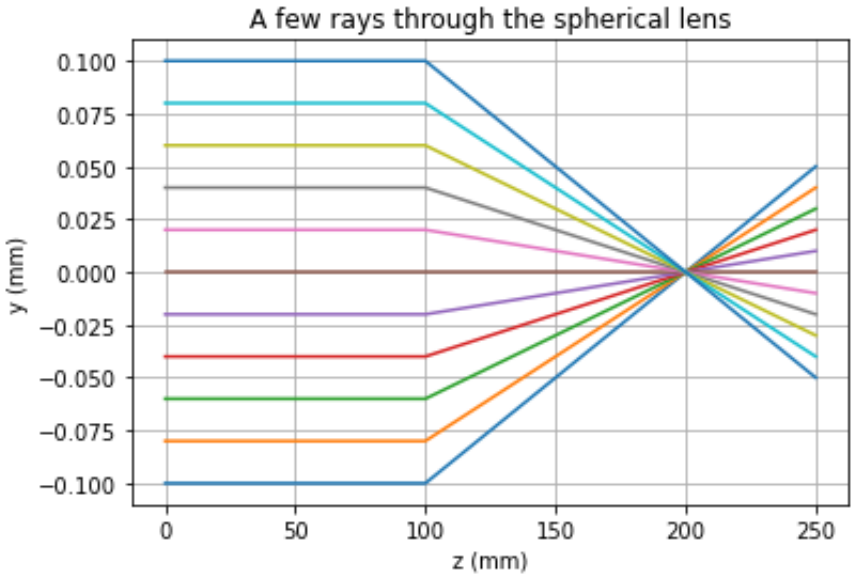

Figure 2 - The trace of a few paraxial rays propagating through the single spherical refracting surface.

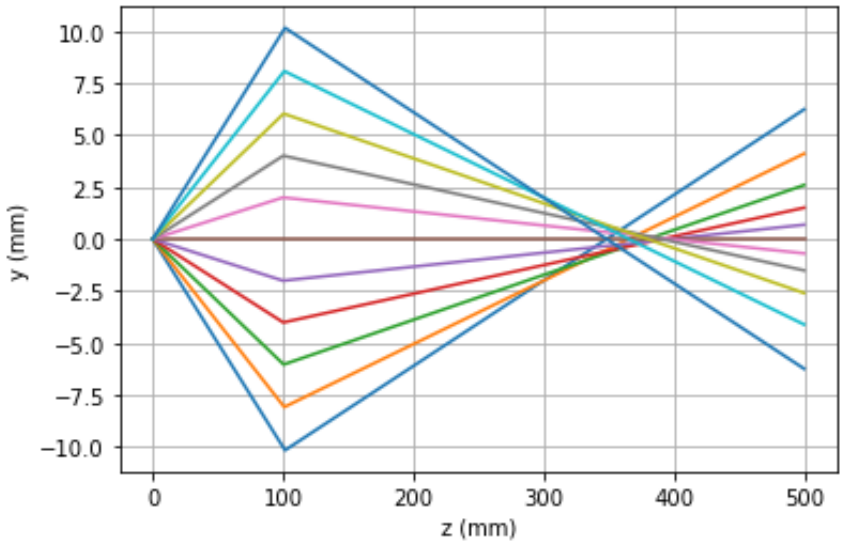

Figure 3 - The trace of a few rays to test the similarity to a thin lens.

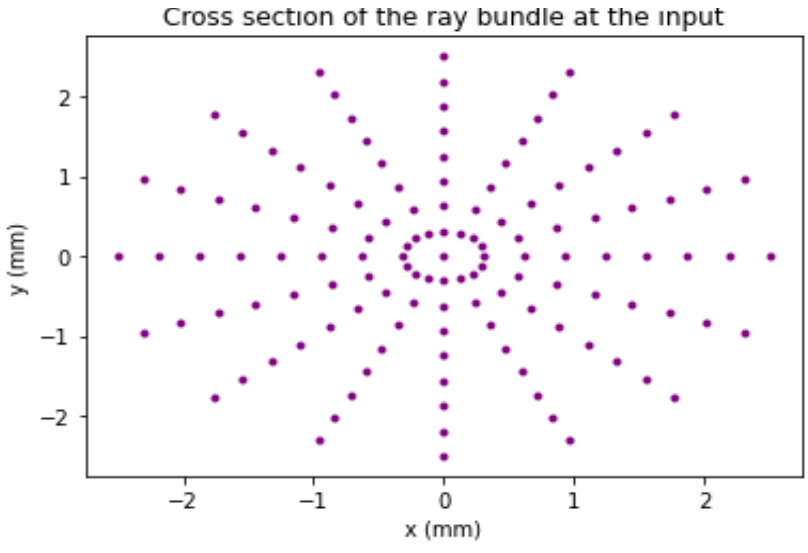

Figure 4 - The spot diagram for the bundle of rays propagated through the single spherical refracting surface.

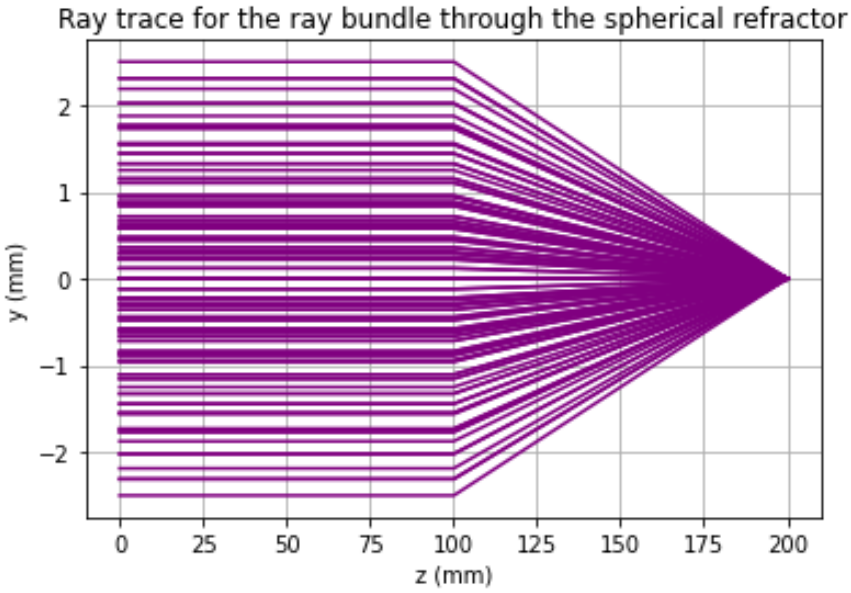

Figure 5 - The trace of the beam through the single spherical refracting surface.

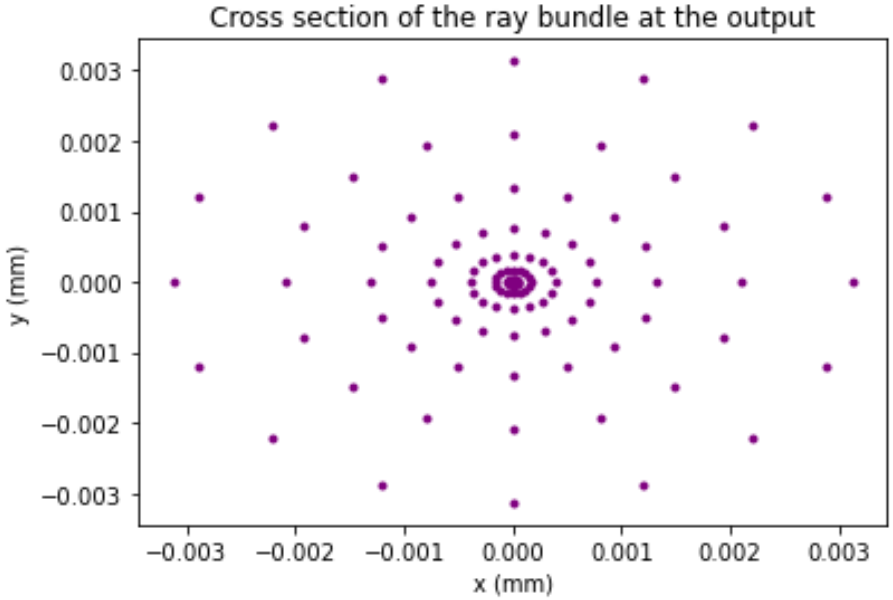

Figure 6 - The spot diagram at the paraxial focus for the single spherical refracting surface.

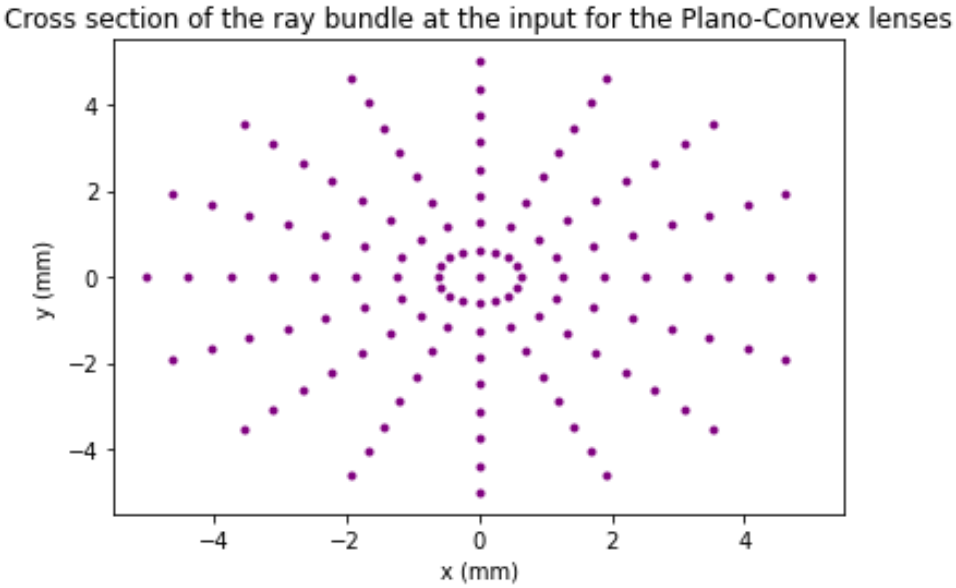

Figure 7 - The spot diagram for the 10 mm diameter beam propagated through the plano-convex lens.

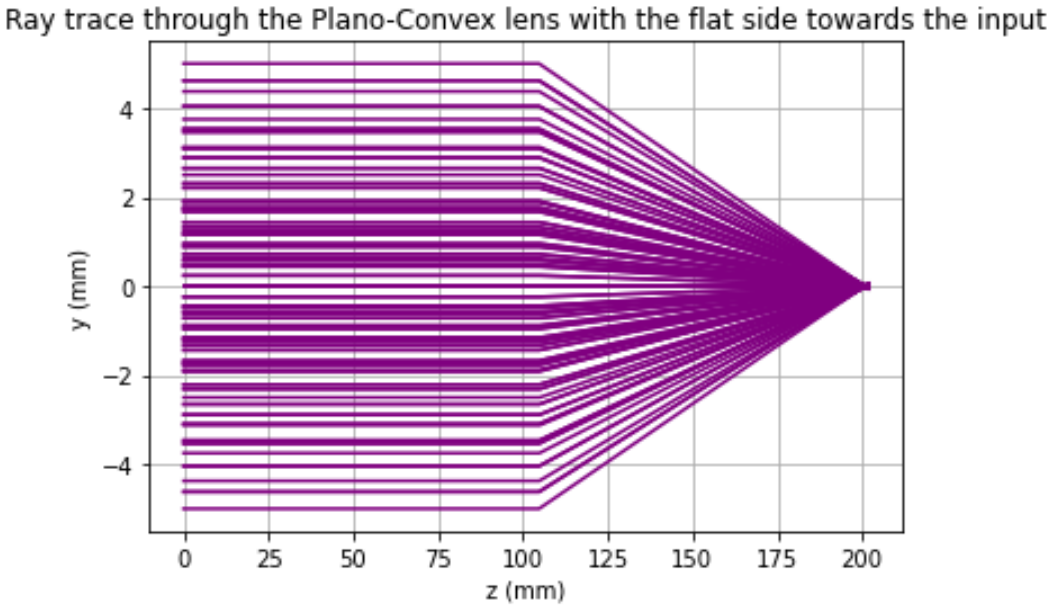

Figure 8 - The trace of the beam through the plano-convex lens, case 1.

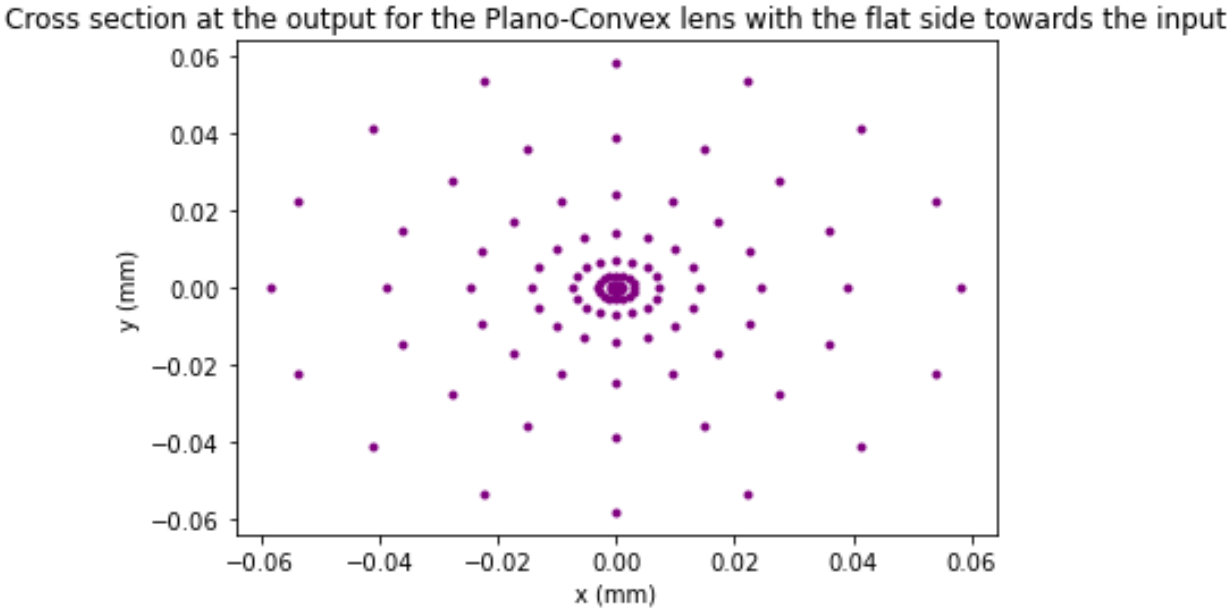

Figure 9 - The spot diagram at the paraxial focal point, case 1.

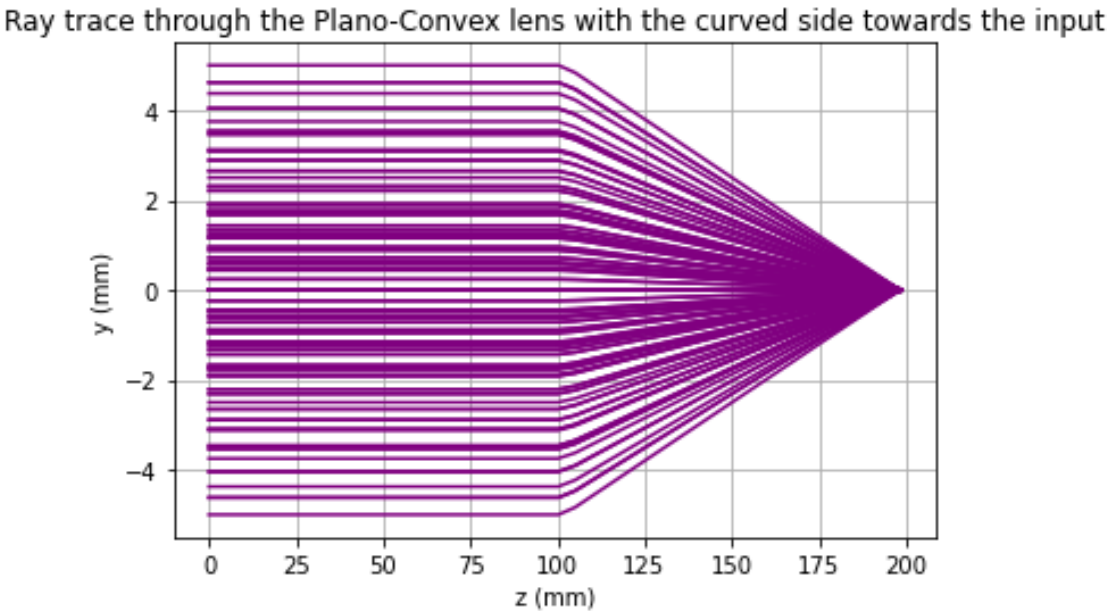

Figure 10 - The trace of the beam through the plano-convex lens, case 2.

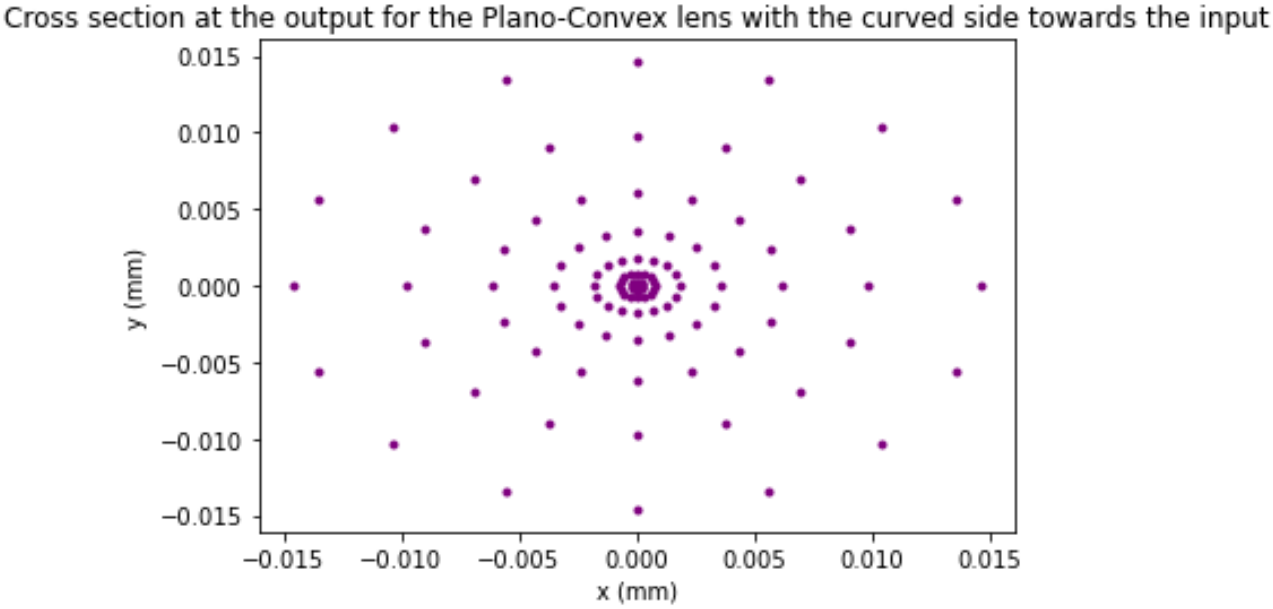

Figure 11 - The spot diagram at the paraxial focal point, case 2.